Electronic Supplementary Material (ESI) for Lab on a Chip.

Supporting Information

A Microfluidic Approach to Micromembrane Synthesis for Complex Release Profiles of Nanocarriers

Jia Nan,[a] Erica Rosella,[a] Estelle Juère,[b] Roxane Pouliot,[c] Freddy Kleitz,[b] Jesse Greener[a,c*]*

[a] Department of Chemistry and Centre de recherche sur les matériaux avancés (CERMA), Université Laval, Québec, Québec G1V 0A6, Canada.

[b] Department of Inorganic Chemistry – Functional Materials, Faculty of Chemistry, University of Vienna, 1090 Vienna, Austria.

[c] Centre de recherche en Organogénèse Expérimentale de l'Université Laval/LOEX, Axe Médecine Régénératrice, Centre de Recherche du CHU de Québec, Université Laval, Québec, QC G1J 1Z4, Canada and Faculté de Pharmacie, Université Laval, Québec, QC G1V 0A6, Canada.

E-mail: jesse.greener@chm.ulaval.ca, freddy.kleitz@univie.ac.at

Sections:

Section S1-Reagents and materials

All reagents were used without further purification. Chitosan (medium molecular weight), phosphate buffered saline tablets (10 mM phosphate buffer, 2.7 mM KCl and 137 mM NaCl, pH 7.4) n-cetyltrimethylammonium bromide (CTAB, 99%), Pluronic F127 ($EO_{106}PO_{70}EO_{106}$, BioReagent), tetraethylorthosilicate (TEOS, 99%), (3-aminopropyl)triethoxysilane (APTS, 99%), succinic anhydride (99%), fluorescein isothiocyanate isomer I, (FITC, ≥ 90%), Triethylamine (TEA), rhodamine B and toluene (anhydrous, 99.8%) purchased from Sigma-Aldrich (Canada). Sodium hydroxide and hydro-chloric acid were purchased from Anachemia (Canada). Polydimethylsiloxane (PDMS, Sylgard184) was provided by Dow corning (Canada). Ammonium hydroxide (28.0% to 30.0%) was obtained from Caledon Laboratory Chemicals (Canada). Ethanol (anhydrous) was supplied by Commercial Alcohols (Canada).

Section S2-Chitosan solution preparation

The chitosan solution was prepared by adding 0.06 g of chitosan flakes into 10 mL de-ionized water, with 1 M HCl solution added dropwise to maintain pH 2 and stirred at room temperature overnight. The pH of the chitosan solution was then adjusted to the desired value by the dropwise addition of 1 M NaOH solution. DI water was added to bring the concentration to the desired value (e.g., to 0.5% w/w or 5 $mg \cdot mL^{-1}$). The resulting chitosan solution was filtered before use with a 0.2 μm syringe filter.

Section S3-Microchannel fabrication and fluid control

The microchannels used in this work were fabricated in polydimethylsiloxane (PDMS) by casting against an X-shape mould with SU-8 photoresist-based features (50 μm height). The mould was designed by computer aided design software (DraftSight™, Dassault systèmes, France). A mixture of liquid PDMS and cross linker at a 10:1 ratio was cast on top of the mold and cured at 70 °C for 4 h. Inlet and outlet holes were added at the end of each arm of the X-channel using needle punch (Figure 1a). Air plasma (PCD-001 Harrick Plasma, Ithaca, USA) activation was used to bond PDMS device to a glass cover slip (VWR, Canada). The device was

then subjected to a brief annealing at 70 °C to strengthen the bonding. Tight fitting metal elbow capillaries were used to connect Teflon tubing to the device access holes. The device was fully transparent, enabling optical characterization. Optical microscope systems with inverted configuration used to observe the membrane included transmission (IX73, Olympus, Canada) and confocal laser scanning (CLSM, FV1200, Olympus, Canada). Images were acquired using a monochrome CCD camera (Lumenera Infinity 3-1 U, Ottawa, Canada). Separate pumps were used to introduce the acidic polymer and the basic aqueous solution and other secondary solutions (e.g., PBS) to the corresponding inlet at respective flow rates, Q_C and Q_B.

Section S4-Solution viscosity and its effect on flow rate ratios

Viscosity measurements were done with Thermogravimetric Analysis (AR-G2, New Castle, DE) in sweep shear rate mode, with a 40 mm diameter 2° cone angle and plate measuring system at 25 °C. Imaging was conducted with an inverted fluorescence microscope (IX73, Olympus, Canada) and by scanning electron microscopy (FEG 250, Quanta, USA).

Large differences in viscosity of co-flowing solutions, higher flow rates of the low viscosity stream had to be applied to balance pressure applied by the high viscosity stream in order to keep their co-flow interface in the middle of the channel. This prevented liquid crossover to wrong outlet, which could cause accumulation of precipitated chitosan downstream and in the outlet tubing, eventually leading to device clogging. Figure S1 shows the viscosity of the NaOH and chitosan solutions. Like other polymer solutions, the chitosan solution is a viscous non-Newtonian liquid, which thins slightly with increasing shear rate. Therefore, in order to keep the interface of laminar co-flow at middle of micro channel, the flow rate of the relatively low viscosity NaOH solution was higher than for the chitosan solution. As the non-Newtonian effects on chitosan solution viscosity were negligible in the range of flow rates used in this work, (Q_T = 2.7 mL·h^{-1} to 13.5 mL·h^{-1}) the Q_B/Q_C ratio was maintained at 26 for all experiments. Lower Q_T values were not possible due to limitations of the pumping system, whereas at higher Q_T values non-Newtonian behaviour became more accentuated, resulting in changes to the position of the co-flow interface.

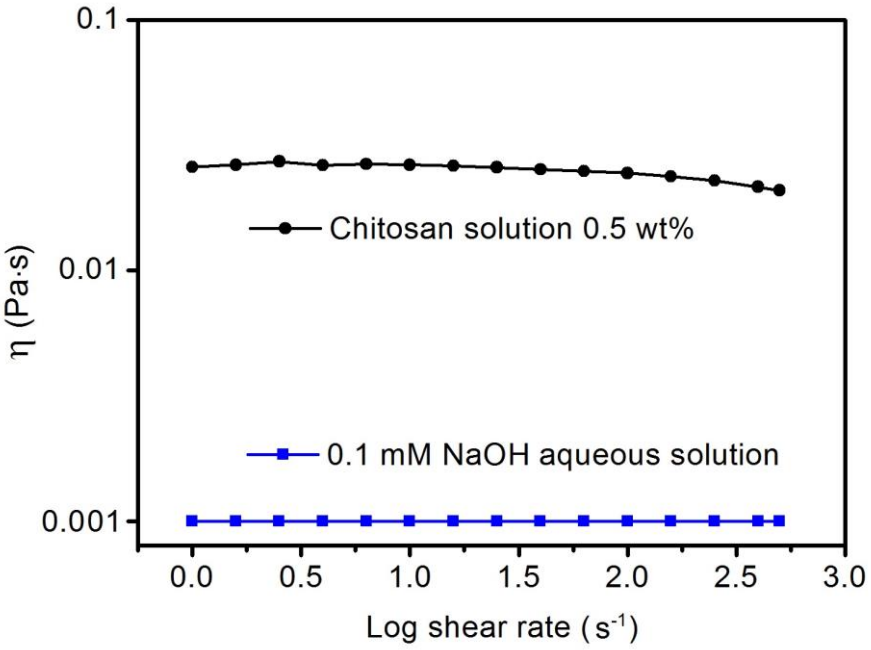

Figure S1. Viscosity versus log shear rate for chitosan solution 0.5% (w/w) in this work (black) and the literature value of 0.1 mM NaOH aqueous solution at pH 10 (blue).

Section S5-Hydrodynamic properties

Using the following formulas, we tabulated hydrodynamic properties in Table S1:

(Average velocity) $$\tilde{v} = \frac{Q}{H \cdot W}$$ (Eqn. S1)

(Reynold's number) $$Re = \frac{\rho \tilde{v} D_H}{\mu}$$ (Eqn. S2)

(Hydraulic diameter) $$D_H = \frac{2W \cdot H}{W + H}$$ (Eqn. S3)

(Shear stress) $$\tau = \frac{6\mu\tilde{v}}{H^2 \cdot W}$$ (Eqn. S4)

where H and W are the height and width of the channel, ρ is the density of liquid, and μ is the viscosity.

Table S1. Calculated hydrodynamic properties of co-flowing chitosan and basic solutions.

		Q ($mL \cdot h^{-1}$)	$\tilde{v}$ ($mm \cdot s^{-1}$)	*Re*	τ (Pa)
Chitosan solution	(a)	0.10	0.556	0.002	1.76
	(b)	0.20	1.111	0.004	3.52
	(c)	0.30	1.667	0.006	5.28
	(d)	0.40	2.222	0.008	7.04
	(e)	0.50	2.778	0.011	8.80
Basic solution	(a)	2.60	14.444	1.375	1.73
	(b)	5.20	28.889	2.751	3.46
	(c)	7.80	43.333	4.127	5.20
	(d)	10.40	57.778	5.503	6.93
	(e)	13.00	72.222	6.878	8.67

Rows (a) – (e) represent different flow condition pairs used in this work.

Section S6-Membrane uniformity and termination

Generally, membranes formed in this work were uniform and had good attachment at the downstream position, e.g. Figure S2a. Errors in membrane termination were not always avoided, e.g. Figure S2b showing the attachment point further downstream than anticipated, with branching in some cases. The reader is directed to a recent paper which focused on the creation of membranes from chitosan, collagen and chitosan/collagen hybrid materials where membrane properties such as uniformity and volume swelling ratio were evaluated as a function of flow rate. [1]

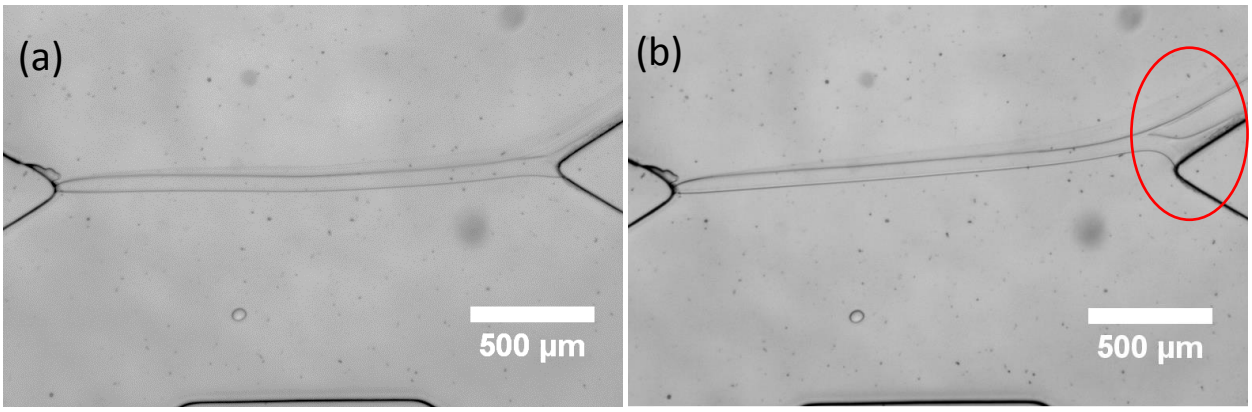

Figure S2. (a) A typical chitosan membrane formed in this work. (b) An example of an error in membrane at the downstream attachment point (red circle).

Section S7-Effect of base solution pH on membrane thickness

Though not explicitly optimized, it was observed that very subtle changes to the base stream pH could have a large effect on membrane thickness as shown in Figure S3.

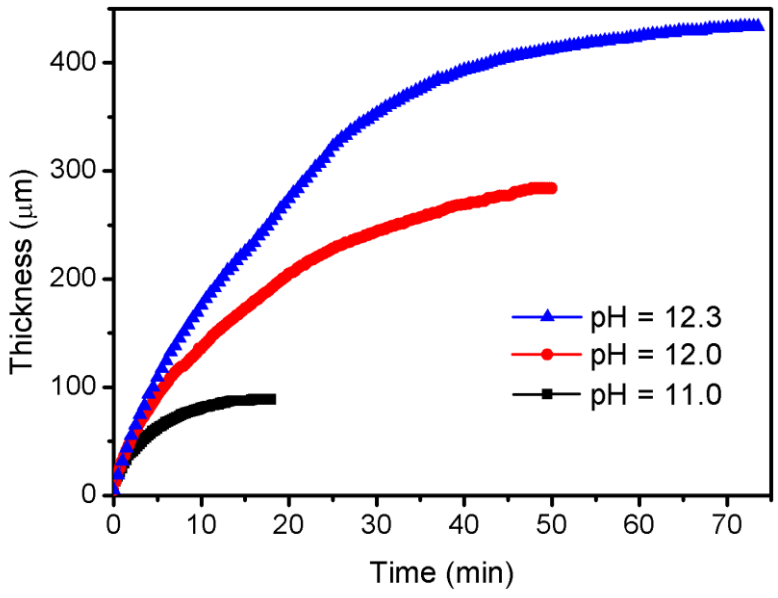

Figure S3. Chitosan membrane growth curves. In all cases, the pH for chitosan solution is 5.5 and Q_T = 2.7 $mL \cdot h^{-1}$.

Section S8-Effect of chitosan solution pH on membrane dissolution rate

The pH of chitosan precursor solutions used during synthesis was shown to have an effect on membrane dissolution rate and dissolution time. Figure S4 plots the trends based on the data in Figure 2d from the main paper. In each case, the dissolution was triggered with a solution of 3.5 flow against the former chitosan polymer solution side, while a PBS buffer was applied against the former basic solution side. The membranes were grown to their full size under specific pH conditions, (3.5, 4.5, and 5.5), which were wider for less acidic chitosan solutions. Therefore, despite increases to dissolution rate with increase synthesis solution pH, the thicker resulting membranes had longer total dissolution times. Faster dissolution rates can decrease dissolution time if the membrane synthesis at different pH values was stopped at a common thickness before reaching full size.

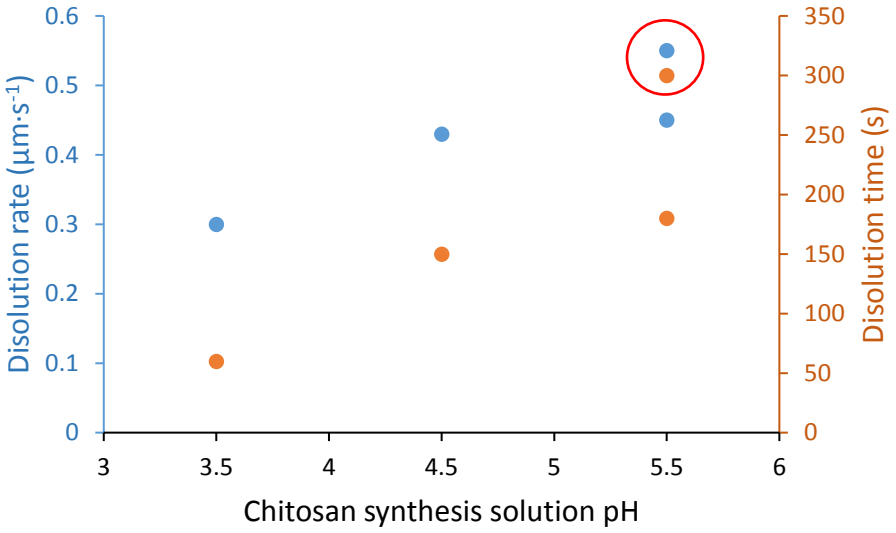

Figure S4. Effect of chitosan solution pH during synthesis on membrane dissolution rate and time after application of pH 3.5 trigger solution. Initial membrane widths were 15, 64, and 80 µm for membranes formed using chitosan solution pH of 3.5, 4,5, and 5.5, respectively at flow rates of 5.4 mL/h and 0.5% w/w. Circled points, used 0.6% w/w to create membranes with 170 µm width.

Section S9-Formation of multi-layer membranes

In the manuscript, three methods for generating multi-layer membranes were explained. (1) In the first, full growth of an initial layer was achieved at high flow rate until growth stopped naturally, then a second layer

was grown by reducing chitosan flow rate injecting. (2) Similar to the first method, a membrane is grown to its full width using a low pH chitosan solution to create the first layer. A secondary chitosan solution with a higher pH, was introduced into the device, causing the membrane to start regrowth, forming the second layer. (3) In the third approach, partial growth was achieved at a low flow rate, followed by periodic interruption and further regrowth by alternating between application of a PBS buffer and slow flowing chitosan solution, respectively. A hybrid approach was also used, in which the interruption-growth cycling used in synthesis method 3 involved alternation between two chitosan solutions containing different disbursed MSNs. Main paper Figures 3c, 3e and 3f used the following chitosan solution combinations. (Figure 3c) MSN_F^+/MSN_R^+; (Figure 3e) MSN_F^+/no MSNs; (Figure 3f) MSN_F^+/MSN_R^+. All methods included an intermediate PBS washing step before growth was restarted to enhance delineation between the layers.

Figure S5a shows the growth curve of a bi-layer membrane using synthesis method 2 from the previous section. An image of the obtained bi-layer system is shown in the figure insert. For the first growth phase (red), the pH of the first chitosan solution and basic solution were 4.5 and 11.0, respectively. The concentration of the chitosan solution was 0.5% w/w and Q_T = 2.7 mL·h^{-1}. After 10 min, the first layer was fully formed and a PBS solution was applied to wash the membrane. Subsequently, a second chitosan solution having a pH of 5.5 was introduced, resulting in the growth of a second membrane layer (growth profile in blue).

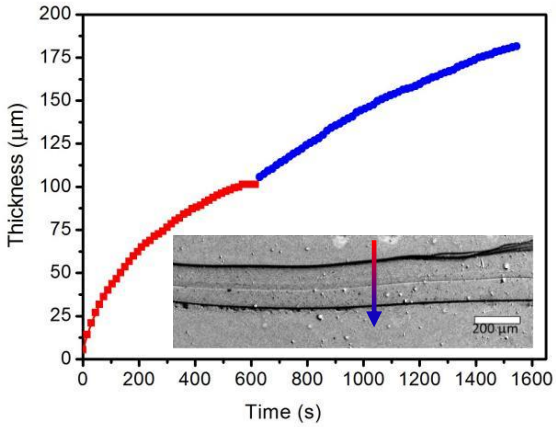

Figure S5. (a) Synthesis of a bi-layer chitosan membrane. Red: pH 4.5, concentration 0.5% w/w, Q_T = 2.7 mL·h^{-1}, blue: pH 5.5, concentration 0.5% w/w, Q_T = 2.7 mL·h^{-1}, Q_C = 0.1 mL·h^{-1}. The inset shows the final bi-layer membrane. The arrow shows the direction of growth with colour corresponding the relevant part of the growth curve.

Section S10- MCM-48 MSN synthesis

MCM-48-type nanoparticles (simply referred as MSNs) were synthesized by following a previously reported procedure. [2] Briefly, 1.0 g of CTAB and 4 g of Pluronic F127 were dissolved in 298 mL of NH_4OH (2.8% w/w)/EtOH = 2.5: 1 (v/v). Then, 3.6 g of TEOS were added and the solution was vigorously stirred (1000 rpm) for 1 min. The mixture was aged in static conditions at room temperature for 24 h and recovered by centrifugation. Afterwards, the white resulting solid was washed twice with 250 mL of water and dried in air at 60 °C overnight. Finally, the resulting product was calcined for 5 h at 550 °C in air.

Table S2. MSN naming convention.

Particle name	Functionalization	Termination
MSN	N/A	N/A
MSN^{+}	APTS	N/A
MSN^{-}	APTS	SA
MSN_F^{+}	APTS	FITC
MSN_R^{+}	APTS	Rhodamine B
MSN_F^{-}	APTS	SA+FITC

Section S11-MSN functionalization

Next, we briefly describe the procedure for functionalizing the particles used in this study.

MSN^{+}: The functionalization of MSNs with APTS follows a previous methodology. [3] Briefly, 200 mg of calcined MCM-48-type nanoparticles were dispersed in 100 mL of dry toluene. The suspension was stirred at 110 °C under N_2 atmosphere for 2 h. Then, 0.2 mL of APTS was added and the grafting continued under stirring and heating overnight. The functionalized product was recovered by centrifugation, washed with ethanol, and dried at 80 °C overnight.

MSN_F^+/MSN_R^+: APTS-functionalized MSNs were coupled with either FITC or rhodamine B according to previous reports. [4] Briefly, 100 mg of FITC or Rhodamine B were dissolved in 25 mL of anhydrous ethanol followed by the addition of 200 mg of APTS-functionalized silica (MSN^+). Then, the suspension was stirred for 24 h at room temperature. The product was recovered by centrifugation and oven dried at 80 °C overnight.

MSN_F^-: Addition of a second terminal functional group, i.e., succinic anhydride (SA), resulted in a competition with fluorophore molecules for access to APTS anchoring sites. [5] To do so, 200 mg of APTS-functionalized MSNs were dispersed in dry toluene at 60 °C under N_2 atmosphere and subsequently 260 mg of SA were added in the presence of TEA (40 mg). After 24 h, the resulting MSN^- was recovered by centrifugation, washed several times with toluene and dried under vacuum overnight at 50 °C for further coupling with FITC. Then, 300 mg of FITC was dissolved in 25 mL of absolute ethanol was combined with 200 mg of MSN^- under stirring at room temperature for 24 h. Finally, the product was recovered by centrifugation and oven dried at 80 °C overnight.

Section S12- MSN characterization

MSN particle size and zeta potential were determined by dynamic light scattering (DLS) using a zetasizer with a scanning angle of 173° (Nano Zetasizer, Malvern Instruments, UK). Fluorescence emission spectra were obtained with a fluorescence spectrophotometer (Cary Eclipse, Agilent). Powder X-ray diffraction measurements were performed using a Siemens D5000 (reflection, θ–θ configuration; Cu Kα: λ = 1.541 Å; 40 kV; 30 mA; 1–8 2θ, step size: 0.02 2θ; 0.02 s/step). The data were analyzed using the Jade software coupled with JCPDS and ICDD databases. N_2 physisorption isotherms were obtained using an Autosorb-1 (Quantachrome Instruments, USA). Before the sorption measurements, the samples were degassed under vacuum at 80 °C. The specific surface area (S_{BET}) was determined using the BET equation in the range 0.05-0.20 and the total pore volume was obtained at $P/P_0 = 0.95$. Pore diameter was estimated from the adsorption branch using non-local density functional theory (NLDFT) method (Autosorb 1.55 software, Quantachrome Instrument, USA) considering the sorption of N_2 at -196 °C in silica with cylindrical pore geometry. Transmission electron microscopy (TEM) images were obtained using a JEM 1230 (JEOL Ltd., Japan). A suspension (4 μL) of the MSNs in methanol was deposited on carbon-coated copper grids prior to the analysis. Thermogravimetric analysis was performed using a Netzsch STA 449C F1 Jupiter (Germany), under airflow of 20 mL min^{-1}, with a heating rate of 10 °C min^{-1}, between 35 and 700 °C.

Figure S6a shows transmission electron microscopy (TEM) image of the unfunctionalized MSNs. Spherical nanoparticles with a narrow particle size distribution were obtained with a particle diameter of about 135 nm. N_2 physisorption (Figure S6b,c) confirmed that the MSNs contained mesopores with sizes of ~3.5 nm, as demonstrated by their type IV isotherm and the respective NLDFT pore size distribution. The highly ordered 3D mesostructured porous network was confirmed by low-angle powder X-ray diffraction (Figure S6d) as observed previously. [2,3]

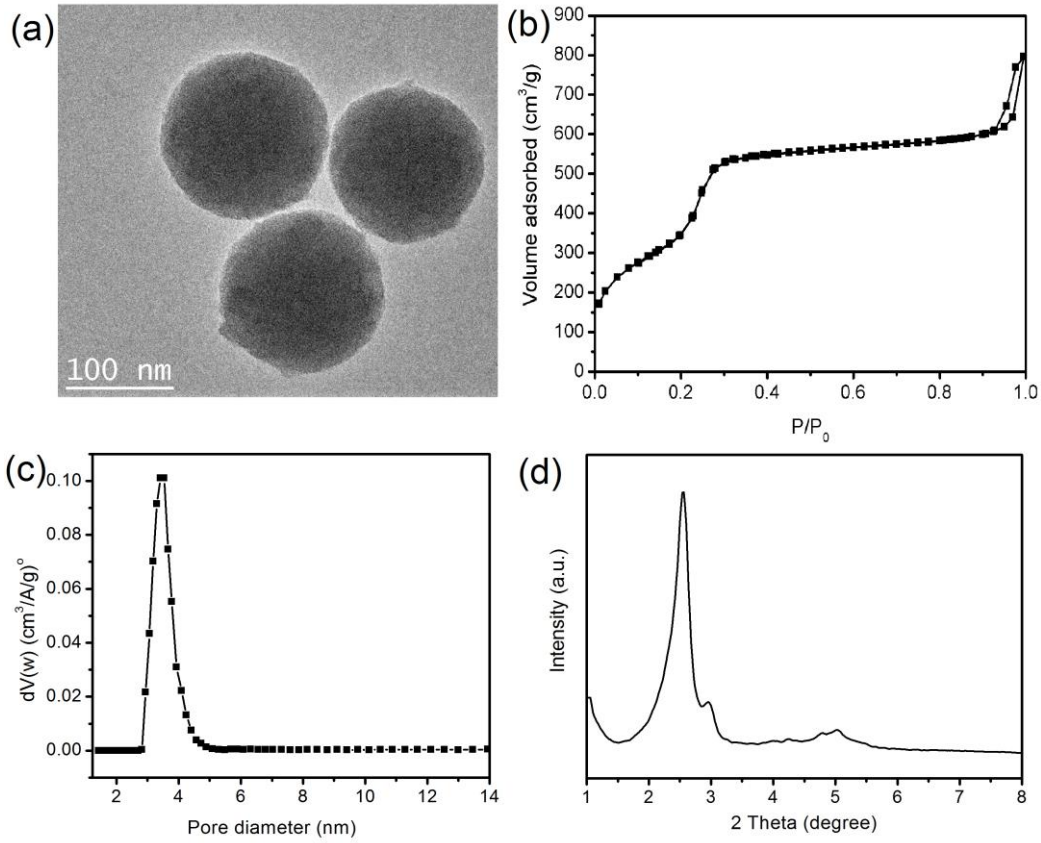

Figure S6. Characterization of unfunctionalized MSNs. TEM image (a) and N_2 adsorption-desorption isotherms curves measured at -196°C (b). Pore size distribution calculated using non-local density functional theory (NLDFT) methods based on cylindrical pore models (c). Low-angle powder XRD pattern (d).

The successful functionalization of the MSNs through covalent grafting was confirmed by thermogravimetric analysis (TGA) (Figure S7a), which indicated that loading amounts of APTS in MSN^+ was approximately 15% by weight, in-line with previous reports. [3-5] The increased weight losses in other samples shown in Figure S7a are consistent with the inclusion of FITC or rhodamine B onto the APTS-functionalized MSNs (MSN_F^+ or MSN_R^+), or the addition of the SA and FITC (MSN_F^-). The zeta potential for MSN_F^- and MSN_F^+ - 36.35 ± 3.03 and 31.63 ± 0.95 mV, respectively. In order to verify that the fluorophores were successfully grafted, fluorescence measurements were acquired on the MSNs. This required removal of loose fluorophore groups. After three ethanol washing/centrifugation cycles (8000 rpm for 30 min), the supernatant was verified to contain no fluorescence bands associated to FITC or Rhodamine B. After this time, the washed MSNs were dispersed in DI water for fluorescence testing. Fluorescence spectroscopy after rinsing showed strong residual fluorescence signals for both fluorophores (Figure S7b) compared to a flat baseline for the unfunctionalized MSNs, confirming the attachment of the fluorophores. As the MSN concentrations were not constant for each measurement, no quantitative information on their relative intensities was obtained.

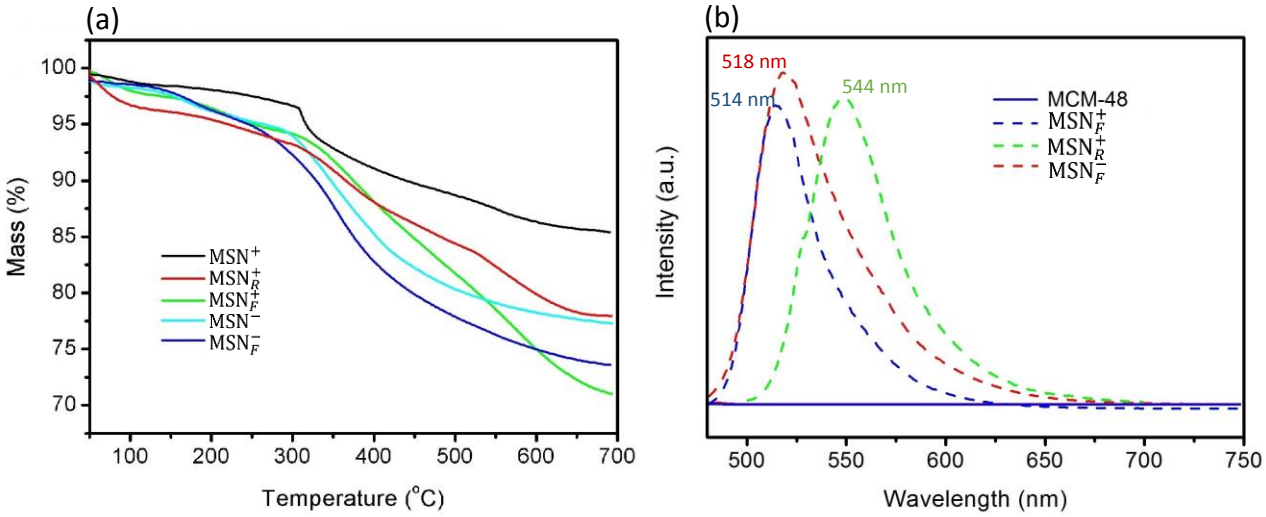

Figure S7. (a) TGA curves of the different functionalized MSNs (see Section S10 for sample descriptions). (b) Fluorescence emission spectra of unfunctionalized MSNs (labelled "MCM-48") and other functionalized particles listed in the figure legend.

Section S13-Stability of membrane-embedded MSNs

A bilayer chitosan membrane containing MSN_F^+ in both layers was prepared, washed with PBS buffer, and photobleached in 6 places. After photobleaching, there was no recovery in the fluorescence signal over 4.5 h,

indicating that the MSNs were immobilized. To test if the laser intensity had an effect on the membrane itself, which prevented the diffusion of the MSNs, a separate experiment was conducted in which a similar bilayer membrane was synthesized, but without MSNs. Again 6 circular areas were photobleached and then a FITC solution was injected into the channel which was absorbed by the membrane rendering it fluorescent. No intensity differences were observed in the membrane in the former laser irradiation locations, suggesting that the photo-bleach process did not damage of alter the structure of chitosan membrane (Figure S8).

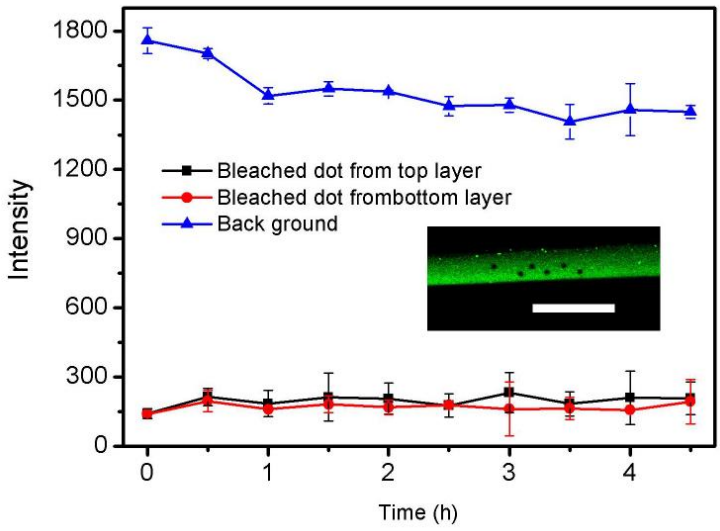

Figure S8. FRAP testing on MSN-APTS-F bilayer membrane formed by method 1 from Section S8 using Q_T = 13.5 mL·h^{-1} then Q_T = 2.7 mL·h^{-1}.

Section S14-MNS concentration and calibration curve

In order to quantify the concentration of MSNs in the membranes and in the effluent after their release, we created a calibration curve using a liquid suspension of nanoparticles at different known MSN concentrations and measured the resulting intensity from the microchannel using the same acquisition parameters used to image fluorescent MSN-loaded membranes. Measurements were conducted in pH = 7.4 to mimic the membrane conditions after exposure to PBS solution following membrane formation. Based on the assumption that fluorescent-labeled MSNs maintained their intensity after becoming embedded in the membrane, the calibration curve enabled the conversion of membrane fluorescence intensity to effluent-phase MSN concentration (Fig. S9).

Based on calibration curve using MSN_F^+ it was discovered that the final MSN concentration in the membrane was close to the value in the precursor polymer solution phase. For a chitosan solution containing 0.5 mg·mL^{-1} MSN_F^+, the membrane concentration was 0.35 mg·mL^{-1}. It was assumed that the type of fluorophore used for functionalization did not affect loading, therefore we normalized MSN_R^+ intensities to the same membrane-bound concentration for multi-layer membranes in Figures 3d-f in the main paper. It is

noted that, MSN concentration in the chitosan solution phase can be another control variable for customization of nano-enabled membranes, though it is not exploited in this proof-of-principle work.

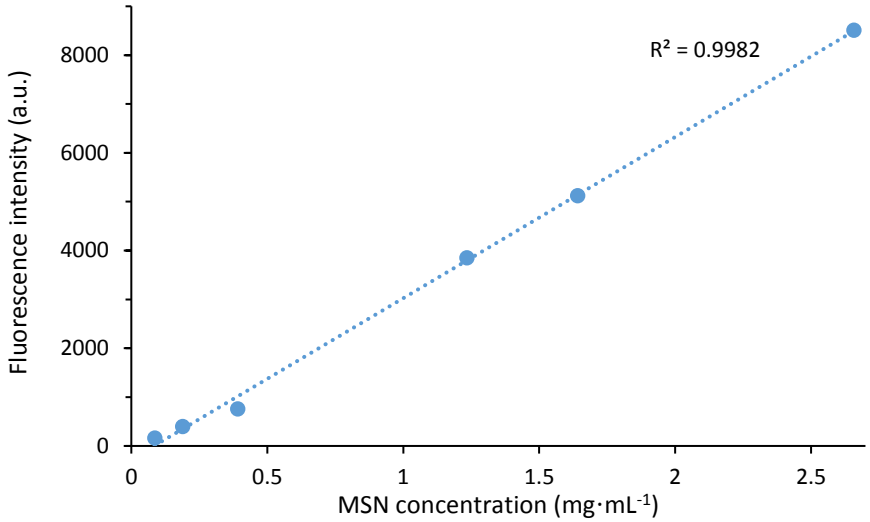

Figure S9. Calibration curve relating known MSN concentration in a solution (pH 7) to its intensity. Acquired using the same fluorescence microscope acquisition parameters used for fluorescence imaging of MSN-loaded chitosan membranes.

Section S15-Cumulative release of multi-functional MSNs from a seven-layer membrane.

Cumulate release profile for seven-layer membrane in Figure 3f in the main manuscript are shown in Figure S10. Flow rate was 1.0 mL/h for a 5.9 pH trigger solution.

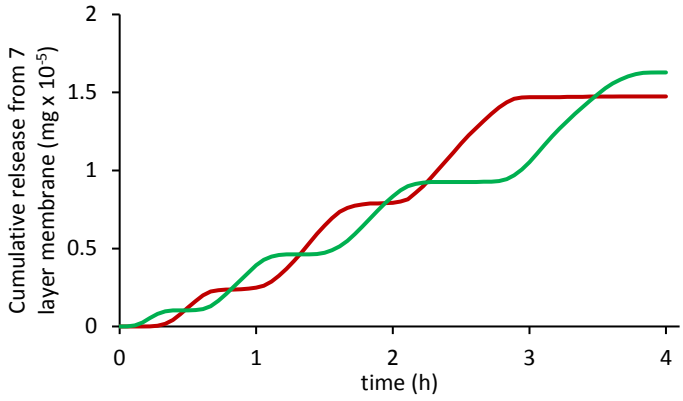

Figure S10. Cumulative release for a 7-layer membrane with alternating MSN_F^+ (green) and MSN_R^+ (red).

Section S15-References

[1] E. Rosella, J. Nan, D. Mantovani, J. Greener, *J. Mater. Sci. Technol.*, **2020**, accepted.
[2] R. Guillet-Nicolas, J. L. Bridot, Y. Seo, M. A. Fortin, F. Kleitz. *Adv. Funct. Mater*. **2011**, 21, 4653.

[3] M. Bouchoucha, M. F. Cote, R. C.-Gaudreault, M. A. Fortin, F. Kleitz. *Chem. Mater*. **2016**, 28, 4243.
[4] C. von Baeckmann, R. Guillet-Nicolas, D. Renfer, H. Kählig, F. Kleitz, *ACS Omega*. **2018**, 3, 17496.
[5] T. Mandal, M. Beck, N. Kirsten, M. Linden, C. Buske. *Sci. Rep*. **2018**, 8, 989.